

169

GMB / ~~ANDERSON~~
CR-128648

NTIS HC \$4.25

E-2712

**OPTIMAL GUIDANCE
FOR THE SPACE SHUTTLE TRANSITION**

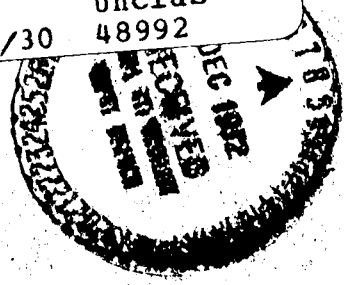
by
Robert F. Stengel

September 1972

(NASA-CR-128648) OPTIMAL GUIDANCE FOR THE SPACE SHUTTLE TRANSITION R.F. Stengel
(Massachusetts Inst. of Tech.) 6 Sep. 1972
43 p CSCL 22C

N73-12905

Unclas
G3/30 48992



**CHARLES STARK DRAPER
LABORATORY**

MASSACHUSETTS INSTITUTE OF TECHNOLOGY

CAMBRIDGE, MASSACHUSETTS, 02139

Reproduced by
**NATIONAL TECHNICAL
INFORMATION SERVICE**
U.S. Department of Commerce
Springfield, VA. 22151

4273

E-2712

OPTIMAL GUIDANCE FOR THE SPACE SHUTTLE TRANSITION

by

Robert F. Stengel

Approved Donald C Fraser Date 5 Sept 1972
D. C. FRASER, ASSISTANT DIRECTOR

Approved David G Hoag Date 6 Sept 72
D. G. HOAG, ASSOCIATE DIRECTOR

Approved Ralph R. Ragan Date 6 Sept 72
R. R. RAGAN, DEPUTY DIRECTOR

ACKNOWLEDGEMENT

This report was prepared under DSR Project 55-40800, sponsored by the Manned Spacecraft Center of the National Aeronautics and Space Administration through Contract NAS 9-10268.

The publication of this report does not constitute approval by the National Aeronautics and Space Administration of the findings or the conclusions contained herein. It is published only for the exchange and stimulation of ideas.

ABSTRACT

A guidance method for the space shuttle's transition from hypersonic entry to subsonic cruising flight is presented. The method evolves from a numerical trajectory optimization technique in which kinetic energy and total energy (per unit weight) replace velocity and time in the dynamic equations. This allows the open end-time problem to be transformed to one of fixed terminal energy. In its ultimate form, "E-Guidance" obtains energy balance (including dynamic-pressure-rate damping) and path length control by angle-of-attack modulation and cross-range control by roll angle modulation. The guidance functions also form the basis for a pilot display of instantaneous maneuver limits and destination. Numerical results illustrate the E-Guidance concept and the optimal trajectories on which it is based.

OPTIMAL GUIDANCE FOR
THE SPACE SHUTTLE TRANSITION

Robert F. Stengel
Charles Stark Draper Laboratory
Massachusetts Institute of Technology
Cambridge, Massachusetts

INTRODUCTION

The transition phase of the space shuttle's return from orbit matches the hypersonic entry phase to the subsonic "cruise" and landing phase. Unlike the neighboring phases, it is characterized by substantial variations in aerodynamic coefficients and stability derivatives, the result of large angle-of-attack changes and flight at supersonic and transonic speeds. As a consequence, transition flight paths are not amenable to the aerodynamic simplifications and analytical solutions which can be applied during entry and terminal-area flight. The importance of transition flight path control is heightened not only by the requirement for unpowered landing approach but by the navigational uncertainties which will prevail as the spacecraft emerges from radio-frequency "blackout." During the latter period of atmospheric entry, inertial estimates of position and velocity will have been degraded by the passage of time since de-orbit platform alignment, and ground-based navigational aids will be obscured by aerothermal ionization. Acquisition of terminal-area radio aids will reduce the navigational uncertainty, and the vehicle may be called upon to perform ranging - and cross-ranging maneuvers at this time.

The central problem of transition flight path control is to manage the mechanical energy that is available following entry in such a way that the destination is reached. Constraints on load factor and dynamic pressure (which can be expressed as functions of kinetic energy, potential energy, and angle of attack) must not be exceeded, and stability and controllability must be maintained. The transition should terminate in a trim-glide flight condition, eliminating the

need for special maneuvering to dissipate excess energy while preserving sufficient energy for a safe landing. The time allowed for transition is open, and the dynamical equations are independent of time.

The significance of energy coupled with the secondary role played by time suggests that a transformation of the variables of motion will simplify the computation of flight paths, with a requisite simplification of the optimization process. Replacing velocity with kinetic energy and time with total energy allows the altitude (potential energy) equation to be eliminated and converts the open end-time problem to one of fixed final energy. The reduced dimension of the trajectory problem increases the plausibility of a dynamic programming solution for real-time applications, and engineering approximations make such an approach feasible for space shuttle guidance.

An energy method for calculating optimal planar trajectories and a 2-dimensional dynamic programming guidance function have been presented recently ¹; in the sections which follow, this development is extended to 3-dimensional flight paths. Equations for steepest-descent optimization using near-optimal stepping of angle-of-attack and roll-angle perturbations are derived. The transition trajectory is initially described by its end points, the starting and final state variables. The trajectory connecting these points must minimize the rate-of-change of dynamic pressure, implicitly limiting maximum load factor and dynamic pressure. This dynamic pressure penalty provides damping of phugoid oscillations through a direct feedback of kinetic-energy rate to angle of attack. In addition to introducing kinetic- and total energy as state- and independent variables respectively, range and cross-range are transformed to polar coordinates centered at the destination. Numerical results illustrate a variety of optimal trajectories, and a 3-dimensional dynamic programming guidance function, which is the basis of the "E-Guidance Law," is demonstrated. The guidance function is shown to be of additional utility in providing a pilot display of instantaneous maneuver limits ("footprint") and destination.

DEVELOPMENT OF EQUATIONS

Transformation of Variables

The equations of motion for the 3-dimensional trajectories considered here make use of the flat-earth approximations — **glide range**, cross-range, and altitude change during the transition maneuver are small compared to the earth's radius, and velocity is decidedly sub-orbital. With the further assumption of an exponential air-density profile ($\rho(H)$), the equations for velocity magnitude (V), flight path angle (γ), altitude (H), range (R), heading angle (ξ), and cross-range (C), which are illustrated in Fig. 1, are

$$\dot{V} = -C_D k e^{-\beta H} V^2/2 - g \sin \gamma \quad (1)$$

$$\dot{\gamma} = C_L k e^{-\beta H} (V/2) \cos \varphi - (g/V) \cos \gamma \quad (2)$$

$$\dot{H} = V \sin \gamma \quad (3)$$

$$\dot{R} = V \cos \gamma \cos \xi \quad (4)$$

$$\dot{\xi} = -C_L k e^{-\beta H} (V/2) \sin \varphi / \cos \gamma \quad (5)$$

$$\dot{C} = V \cos \gamma \sin \xi \quad (6)$$

The control variables in these point-mass equations are roll angle (φ) and angle of attack (α); α enters through the aerodynamic coefficients for lift and drag (C_L and C_D). Additional variables are the inverse scale height of air density (β), the gravitational constant (g), and the density ratio per unit length ($k = S \rho_0 / m$), which combines reference area (S), vehicle mass (m), and reference air density (ρ_0).

It is convenient to transform range and cross-range into a distance from the destination and an azimuth angle, which is referenced to the original heading angle. Denoting final values by the subscript "f", the range-to-go and cross-range-to-go are

$$R_{go} = R_f - R, \quad C_{go} = C_f - C \quad (7, 8)$$

while the distance-to-go (D_{go}) and destination azimuth angle (η) are

$$D_{go} = [R_{go}^2 + C_{go}^2]^{1/2} \quad (9)$$

$$\eta = \tan^{-1} (C_{go} / R_{go}) = \cos^{-1} (R_{go} / D_{go}) \quad (10)$$

The differential equations for the time rate-of-change of D_{go} and η , using eq. 4, 6, 7, 8, 9, 10 are

$$\begin{aligned} \dot{D}_{go} &= (C_{go} \dot{C}_{go} + R_{go} \dot{R}_{go}) / (C_{go}^2 + R_{go}^2)^{1/2} \\ &= -V \cos \gamma \cos \eta (\tan \eta \sin \xi + \cos \xi) \end{aligned} \quad (11a)$$

$$\begin{aligned} \dot{\eta} &= (R_{go} \dot{C}_{go} - C_{go} \dot{R}_{go}) / (R_{go}^2 + C_{go}^2) \\ &= -V \cos \gamma (\sin \xi - \tan \eta \cos \xi) / D_{go} \cos \eta (1 + \tan^2 \eta) \end{aligned} \quad (12a)$$

The $\cos \eta$ divisor and $\tan \eta$ terms lead to computational difficulties for $\eta = \pm 90^\circ$; however, the equations can be rewritten as

$$\begin{aligned} \dot{D}_{go} &= -V \cos \gamma (\sin \eta \sin \xi + \cos \eta \cos \xi) \\ &= -V \cos \gamma \cos (\eta - \xi) \end{aligned} \quad (11b)$$

$$\begin{aligned} \dot{\eta} &= -V \cos \gamma (\cos \eta \sin \xi - \sin \eta \cos \xi) / D_{go} \\ &= V \cos \gamma \sin (\eta - \xi) / D_{go} \end{aligned} \quad (12b)$$

As indicated by Fig. 1, the term $(\eta - \xi)$ is the angle between the line-of-sight to the destination and the longitudinal axis of the vehicle,* i. e., the horizontal "look angle" or azimuth-to-go (A_{go}). The solution for horizontal position is seen to be independent of the actual values of η and ξ , relying only on their difference for dynamic effect.

The specific kinetic energy, or kinetic energy per unit weight, is

$$K = V^2 / 2g, \quad (13)$$

which possesses the time-derivative,

* assuming zero sideslip angle

$$\dot{K} = V \dot{V} / g ; \quad (14)$$

hence, V and \dot{V} can be replaced by K and \dot{K} in the system equations, yielding the following set :

$$\dot{K} = -C_D k e^{-\beta H} (2gK^3)^{1/2} - (2gK)^{1/2} \sin \gamma \quad (15)$$

$$\dot{\gamma} = C_L k e^{-\beta H} (gK/2)^{1/2} \cos \varphi - (g/V) \cos \gamma \quad (16)$$

$$\dot{H} = (2gK)^{1/2} \sin \gamma \quad (17)$$

$$\dot{D}_{go} = -(2gK)^{1/2} \cos \gamma \cos (\eta - \xi) \quad (18)$$

$$\dot{\xi} = -C_L k e^{-\beta H} (gK/2)^{1/2} \sin \varphi / \cos \gamma \quad (19)$$

$$\dot{\eta} = (2gK)^{1/2} \cos \gamma \sin (\eta - \xi) / D_{go} \quad (20)$$

Since these equations have no explicit dependence on time, their number can be reduced by redefining the independent variable to be one or a combination of the state variables. The new independent variable should be monotonic in time on a typical trajectory to avoid singular points and multi-valued control histories. Occurrence of a phugoid oscillation (the long-period interchange of kinetic- and potential energies) could prevent the first 3 variables from individually meeting this requirement, while choice of one of the remaining 3 variables introduces an artificial dependence on lateral state in the longitudinal equations. As shown previously,¹ the specific total energy, or total energy per unit weight,

$$E = K + H , \quad (21)$$

meets the requirements for a new independent variable. E must be monotonic in gliding flight, as

$$\dot{E} = \dot{K} + \dot{H} , \quad (22a)$$

which, from eq. 15 and 17 is

$$\dot{E} = -C_D k e^{-\beta H} (2gK^3)^{1/2} \quad (22b)$$

The individual terms on the right side of eq. 22 are always positive; hence, total energy is always dissipated by aerodynamic drag. The derivatives with respect to the new independent variable are

$$d() / dE = [d() / dt] / \dot{E} \equiv ()' \quad (23)$$

and the differential equation for either K' or H' can be eliminated in favor of eq. 21. Eliminating the H' equation, the dynamic equations become

$$K' = 1 + \sin \gamma / C_D \mu \quad (24)$$

$$\gamma' = (-C_L \cos \varphi + \cos \gamma / \mu) / 2 C_D K \quad (25)$$

$$D'_{go} = \cos \gamma \cos (\eta - \xi) / C_D \mu \quad (26)$$

$$\xi' = C_L \sin \varphi / 2 C_D K \cos \gamma \quad (27)$$

$$\eta' = -\cos \gamma \sin (\eta - \xi) / D_{go} C_D \mu \quad (28)$$

where μ is a measure of the aerodynamic forces,

$$\mu = k e^{-\beta H} K = q / (W/S) \quad (29)$$

with q = dynamic pressure and $W = mg$.

Several simplifications might be considered at this time. $\dot{\gamma}$ has been found to be negligible during transition maneuvers², including those with a rapid change in α ; setting the left side of eq. 25 to zero allows the transcendental solution

$$\cos \gamma = C_L \mu \cos \varphi \quad (30)$$

This approximation leads to computational difficulties in horizontal flight¹ but could be of value for some applications. Replacing eq. 28 with a relation for A'_{go} and assuming that A'_{go} is negligible yields a transcendental solution for roll angle,

$$\sin \varphi = -2 \sin A_{go} / D_{go} \cos^2 \gamma C_L k e^{-\beta H}, \quad (31)$$

which should be valid until D_{go} becomes very small, at which time the assumption can be violated by significantly different ξ' and η' ; the magnitude of the right side of eq. 31 can then exceed 1. This result suggests a roll control law which steers to the destination while minimizing the rate-of-change of the azimuth-to-go. A third simplification, which is adopted for the remainder of the paper, is that the flight path angle can be assumed small during the transition, leading to $\cos \gamma \simeq 1$ and $\sin \gamma \simeq \gamma$. This assumption is borne out by previous results^{1,2}, and it provides a modest reduction in the number and complexity of the partial derivatives required for variational optimization. Equations 24 to 28 can now be expressed as

$$\underline{x}' = \underline{f}(\underline{x}, \alpha, \varphi) \quad (32)$$

where $x_1 = K$, $x_2 = \gamma$, $x_3 = D_{go}$, $x_4 = \xi$, $x_5 = \eta$, and

$$f_1 = 1 + x_2 / C_D \mu \quad (33)$$

$$f_2 = [-C_L \cos \varphi + 1 / \mu] / 2 C_D x_1 \quad (34)$$

$$f_3 = \cos(x_5 - x_4) / C_D \mu \quad (35)$$

$$f_4 = C_L \sin \varphi / 2 C_D x_1 \quad (36)$$

$$f_5 = -\sin(x_5 - x_4) / x_3 C_D \mu \quad (37)$$

Eighteen of the 35 partial derivatives of \underline{f} with respect to \underline{x} , α , and φ are non-zero. Assuming that C_{LM} and C_{DM} are negligible, these partial derivatives (which will be used in the next section) are

$$f_{1x_1} = -x_2 (\beta + 1/x_1) / C_D \mu \quad (38)$$

$$f_{1x_2} = 1 / C_D \mu \quad (39)$$

$$f_{2x_1} = [C_L \cos \varphi - (2 + \beta x_1) / \mu] / 2 C_D x_1^2 \quad (40)$$

$$f_{3 x_1} = -\cos A_{go} (\beta + 1/x_1) / C_D \mu \quad (41)$$

$$f_{3 x_4} = \sin A_{go} / C_D \mu \quad (42)$$

$$f_{3 x_5} = -f_{3 x_4} \quad (43)$$

$$f_{4 x_1} = -C_L \sin \varphi / 2 C_D x_1^2 \quad (44)$$

$$f_{5 x_1} = \sin A_{go} (\beta + 1/x_1) / x_3 C_D \mu \quad (45)$$

$$f_{5 x_3} = \sin A_{go} / x_3^2 C_D \mu \quad (46)$$

$$f_{5 x_4} = \cos A_{go} / x_3 C_D \mu \quad (47)$$

$$f_{5 x_5} = -f_{5 x_4} \quad (48)$$

$$f_{1 \alpha} = -x_2 C_{D\alpha} / C_D^2 \mu \quad (49)$$

$$f_{2 \alpha} = [-C_{L\alpha} \cos \varphi + (C_L \cos \varphi - 1/\mu) C_{D\alpha} / C_D] / 2 C_D x_1 \quad (50)$$

$$f_{3 \alpha} = -\cos A_{go} C_{D\alpha} / C_D^2 \mu \quad (51)$$

$$f_{4 \alpha} = (C_{L\alpha} \sin \varphi - C_L C_{D\alpha} / C_D) / 2 C_D x_1 \quad (52)$$

$$f_{5 \alpha} = \sin A_{go} C_{D\alpha} / x_3 C_D^2 \mu \quad (53)$$

$$f_{2 \varphi} = C_L \sin \varphi / 2 C_D x_1 \quad (54)$$

$$f_{4\phi} = C_L \cos \phi / 2 C_D x_1 \quad (55)$$

where $A_{go} = \eta - \xi$. The partial derivatives are seen to be well-behaved except at the destination ($x_3 = 0$) or in flight at vanishing dynamic pressure ($\mu = 0$), in which case energy dissipation is negligible.

Equations and Methodology of Optimization

Optimization of the 3-dimensional dynamic equations proceeds according to standard methods of variational calculus. The control which minimizes a cost function consisting of integral and terminal penalties is to be found. The cost function, augmented by the dynamic constraints (eq. 32), is

$$J = (\underline{x}_f - \underline{x}_D)^T \underline{Q} (\underline{x}_f - \underline{x}_D) + \int_{E_0}^{E_f} \{ \mathcal{L}(\underline{x}, \underline{u}) + \underline{\lambda}^T [\underline{f}(\underline{x}, \underline{u}) - \underline{x}'] \} dE, \quad (56)$$

$E_0 > E_f$,

where the end points are fixed, \underline{Q} is a constant, diagonal matrix weighting the squared-error between the achieved- and desired final state, \mathcal{L} is a penalty function whose integral must be minimized, $\underline{\lambda}$ is the vector adjoint of \underline{x} , and the control vector is

$$\underline{u} = \begin{bmatrix} \alpha \\ \phi \end{bmatrix} \quad (57)$$

The state vector is a function of E through eq. 32, while $\underline{\lambda}(E)$ is found from

$$\underline{\lambda}'(E) = - \underline{f}_x^T(E) \underline{\lambda}(E) - \underline{\mathcal{L}}_x^T(E) \quad (58)$$

with

$$\underline{\lambda}(E_f) = 2 \underline{Q} (\underline{x}_f - \underline{x}_D) \quad (59)$$

Having obtained a trajectory from eq. 32 with an initial control profile $\underline{u}(E)$, the angle-of-attack and roll-angle histories are improved on succeeding iterations by the perturbation,

$$\delta \underline{u}(E) = \epsilon \begin{bmatrix} (\mathcal{L}_\alpha + \lambda \underline{T}_f \underline{\alpha}) \\ \sigma (\mathcal{L}_\varphi + \lambda \underline{T}_f \underline{\varphi}) \end{bmatrix} = \epsilon \begin{bmatrix} \delta \alpha (E) \\ \sigma \delta \varphi (E) \end{bmatrix} \quad (60)$$

where ϵ and σ are near-optimal step-sizes obtained by a 2-dimensional search of $J(\epsilon, \sigma)$.

The cost-function search for near-optimal ϵ and σ is sequential. Choosing the initial roll/angle-of-attack ratio, σ_0 , to be 1, a quadratic approximation, $\tilde{J}(\epsilon, \sigma_0)$, is found by evaluating the costs of 3 trajectories with $\epsilon = 0, \epsilon_0$, and $2\epsilon_0$. If $\tilde{J}(\epsilon_0, \sigma_0) > \tilde{J}(0, \sigma_0)$, the step-size sequence is $\epsilon = 0, \epsilon_0/2$, and ϵ_0 . The first search is completed by finding ϵ^* , the α -step which minimizes $\tilde{J}(\epsilon, \sigma_0)$. The minimum in $\tilde{J}(\epsilon^*, \sigma)$ is then evaluated by a quadratic fit in σ , with $\sigma = 0, \sigma_0$, and $2\sigma_0$ (or $\sigma = 0, \sigma_0/2, \sigma_0$, as above), σ^* , the minimizing φ/α ratio, and ϵ^* are then used in eq. 60 to perturb the control profile and to compute the final trajectory of the iteration. On succeeding iterations, ϵ_0 and σ_0 equal the minimizing values from the previous iteration.

Terminal distance corrections are most readily made by varying the control early in the trajectory, yet some difficulty has been experienced in achieving this obvious correction from the optimization equations.¹ The problem has been overcome by imposing ramp-function weighting on ϵ when the terminal distance error is large. The ramp function equals 1 at E_0 and 0 at E_f ; therefore, control corrections are attenuated as the terminal point is approached. This allows large changes in terminal D_{go} with little change in final V, γ , and ξ , which are primarily determined by the control profile in the latter portion of the flight.

The integral penalty function (\mathcal{L}) contains terms which enforce control boundaries and which introduce trajectory damping. Angle-of-attack limits beyond which quadratic penalties occur, are academic for the present results, as none of the optimal profiles shown here follow an α boundary. The trajectory damping term penalizes the rate-of-change of dynamic pressure (q), which is

$$q' = q [(\beta x_1 + 1) f_1 - \beta x_1], \quad (61)$$

where $q = \rho_0 e^{-\beta(E - x_1)g x_1}$, and f_1 is found from eq. 33. The penalty function is then

$$\mathcal{L} = c q'^2, \quad c < 0, \quad (62)$$

which has the partial derivatives

$$\begin{aligned} \mathcal{L}_{x_1} = & 2 c q q' \{ (\beta + 1 / x_1) [(\beta x_1 + 1) f_1 - \beta x_1] \\ & + [\beta (f_1 - 1) + (\beta x_1 + 1) f_{1x_1}] \} \end{aligned} \quad (63)$$

$$\mathcal{L}_\alpha = 2 c q q' (\beta x_1 + 1) f_{1\alpha} \quad (64)$$

Equation 61 shows that \mathcal{L} is primarily a kinetic-energy-rate penalty which is weighted by air density. The damping penalty establishes a direct relationship between acceleration along the velocity vector and α , and it is independent of both ϕ and the other state variables. The principle of damping the trajectory by longitudinal motions alone is extended to the E-Guidance method, which is presented later in this paper.

In the numerical results which follow, terminal K , γ , and D_{go} errors are weighted in eq. 59, and η_{go} is open. The transformation from t and V to E and K provides implicit weighting of terminal altitude error, as E_f is fixed, and the K_f error is minimized; hence, from eq. 21, H_f error is minimized as well. The use of polar coordinates to describe horizontal position allows the most important navigational error to be described by one terminal variable (D_{go_f}) rather than two (R_{go_f} , C_{go_f}). The final heading angle, ξ_f , must be specified for the terminal maneuver which aligns the vehicle with the runway, and a quadratic ξ_f penalty is demonstrated here. In the real-time guidance problem, the final heading is more readily handled by re-targeting the terminal point from the nominal aim point to a point of tangency on a heading alignment cylinder of radius, D_H . The final heading in the transition phase is then $\pm 90^\circ$ from the azimuth (η_H) to the nominal aim point.

APPLICATION TO TRANSITION FLIGHT PATHS

The lift, drag, and mass characteristics upon which the following optimal trajectories are based pertain to a delta-winged configuration for the space shuttle orbiter.³ The maximum hypersonic L/D of 2.1 occurs at $\alpha = 13.8^\circ$, while the subsonic $L/D_{\max} = 4.3$ and occurs at $\alpha = 8.4^\circ$. The transition phase begins in the hypersonic regime ($M = 8.26$, $H = 150,000$ ft, $\gamma = 0^\circ$) and ends in a subsonic trim glide ($M = .9$, $H = 40,000$ ft, $\gamma = -18^\circ$). Initial specific total energy (1.15×10^6 ft) consists primarily of kinetic energy, whereas the terminal specific energy (5.18×10^4 ft) is largely due to the terminal altitude.

The trajectories demonstrated in this section end at ranges of 200- to 402 nmi from the starting point, and cross-range varies from 50- to 150 nmi (detailed results for 2-dimensional, planar trajectories are presented in Ref. 1). The data are computed using the flat-earth model presented in an earlier section and are compared briefly with round(non-rotating)-earth trajectories for the same control profiles, which are scheduled as functions of E . Initial condition- and mass-variation effects are presented, as are the variations due to a constrained final heading angle.

General Characteristics of the Trajectories

Given the nominal initial conditions described above, the space shuttle orbiter can fly to any destination within the "footprint" illustrated in Fig. 2. This near-optimal envelope of reachable points has been determined by modulating α (as a function of Mach number) such that the lift-drag ratio is always maximized. The roll angle (ϕ) has been held constant until a heading angle (ξ) of 90° is obtained, at which time ϕ is nulled. The vehicle descends to the nominal specific energy of 5.18×10^4 ft, corresponding to final velocities and altitudes of about 800 fps and 41,500 ft. Peak dynamic pressures (q) on the trajectories to the locus of terminal points indicated in the figure are large, the result of the uncontrolled phugoid oscillations induced by the non-equilibrium initial flight condition. These peaks can be substantially reduced by active control, at the cost of a slight reduction in maximum horizontal path length, which is measured along the dashed lines of Fig. 2. The round-earth model used in generating this footprint produces longer range and lower q_{\max} than the corresponding flat-earth trajectories.

Fifteen optimal trajectories within this footprint have been computed; their ground tracks are illustrated in Fig. 3. The zero-cross-range terminal point at 402-nmi-range is a flat-earth L/D_{\max} trajectory, whose round-earth counterpart

has 20-nmi-greater range. The remaining 14 cases were computed with dynamic-pressure-rate damping. The preponderance of $q_{\max} = 187$ psf in Fig. 3 indicates that, in each case, the terminal q is the maximum value. Maximum load factor occurs at or near the starting point of each trajectory; hence, those cases with shorter path length have commensurately higher maximum load.

A summary of energy distribution on the transition flight paths is offered by the altitude-velocity (H-V) profiles of Fig. 4, which effectively plot potential energy against kinetic energy (eq. 13 and 21). The contours of constant E and q provide a background against which the most significant dynamic effects of terminal point can be evaluated. Flight to short-range terminal points necessitates early deceleration, which is obtained by increasing α . This not only leads to increased drag but to increased lift as well, causing altitude to increase. Roll switching, of the sort used for Apollo entry control or as recently suggested for the low L/D , heat-constrained phase of the shuttle entry⁴, could prevent the altitude increase, although this characteristic does not constitute a guidance problem. The reduction in dynamic pressure has a more direct effect on attitude control using aerodynamic surfaces - the return to low q results in sluggish response to surface deflection, introducing a possible need for continued use of the reaction control thrusters used earlier in the entry and during orbital flight. Matching the H-V profiles with their corresponding ground tracks in Fig. 3, the energy balance during transition is seen to be a stronger function of path length than of the amount of path curvature. For the 200-nmi case shown in Fig. 4, the phugoid oscillation which proceeds from the altitude increase is well-damped by α modulation during the ensuing flight. Increasing the path length to the terminal point forces a descent into regions of higher dynamic pressure. For a given specific energy, the ratio of kinetic-to-potential energy increases as terminal distance increases. This is less of an energy effect than a minimization of the product $C_D \mu$, which forms the denominator of $\partial D_{go} / \partial E$ (eq. 26) and, therefore, has an inverse effect on the final path length. The H-V profiles coalesce into a single curve as the final point is approached.

Details of 4 trajectories which constitute the extremes of the 9 out-of-plane cases considered in this section are presented in Fig. 5 to 7: high- and low terminal ranges are combined with high- and low cross-ranges. The control angles (Fig. 5) and position variables (Fig. 6) illustrate the obvious separation of α and ϕ control functions. Angle of attack is principally an energy and distance control, while ϕ determines the lateral state.

The path length trends evident in H-V can be seen again in α (Fig. 5a) and D_{go} (Fig. 6a). The α - profiles for long path length (R = 390 nmi, C = 50 nmi and R = 350 nmi, C = 150 nmi) are virtually identical, as are the D_{go} profiles. In both cases α remains close to the L/D_{max} profile except at the end points. Variation at the final point is required to match the specified V_f and H_f . An initial α - "pop-up" is executed in an attempt to minimize the inevitable dynamic pressure peak (Fig. 7a) associated with the long-distance transition. The phugoid oscillation of the high-range, high-cross-range case is especially evident in the q history, suggesting that further iteration during the optimization might be fruitful; however it must be recalled that these oscillations are unavoidable in the range-optimum case, and this case approaches the near-optimal footprint (Fig. 3) more closely than any of the others.

The correspondence between φ and A_{go} shown by Fig. 5b and 6b is clear -- an overlay of the 2 figures shows a remarkable similarity not only of general shape but of magnitude as well (note that the polarity is opposite with the sign conventions used here). The similarity is explained by the fact that the rate-of-change of A_{go} is small; thus, by eq. (31), $\sin \varphi$ is proportional to $\sin A_{go}$. The undulations in φ for the 200-nmi-range cases are related to similar features in the α - profiles because the φ - A_{go} proportionality is weighted by C_L , in turn a function of α .

Dynamic pressure (Fig. 7a) shows the trends predicted by the H-V profile. The high-range, high cross-range and high-range, low cross-range profiles are similar throughout the energy interval, the low-range, low cross-range case has uniformly low q, and the low-range, high cross-range case begins with the low q characteristic of early energy dissipation and switches to higher q for path extension once the vehicle's heading change has brought A_{go} to a low value. The first 2 cases show initial load factors below 1 "g" (Fig. 7b) as the spacecraft conserves kinetic energy to establish a near-minimum $C_D \mu$ for long distance (see earlier discussion) while reducing the first q peak. The remaining 2 cases have low q, but load factor is high, a result of the high α required for distance control. Although one might normally equate low q with low load factor, these 4 cases indicate just the opposite. As a consequence, trajectories which minimize one parameter do not necessarily minimize the other, and an attempt to minimize both at once could be confounded by competing integral penalties. Round-earth trajectories flown with the α - φ control histories used in these 4 cases have range increases of 7 to 19 nmi and cross-range increases of 2 to 4 nmi. Dynamic

pressure peaks occurring during the flight (not at the final point) decrease from 0 to 42 psf.

Comparing these results with those for in-plane¹ trajectories, it is found that α , q , and load factor trends are not materially altered by path curvature; path length is the distinguishing parameter for both in-plane and out-of-plane motion. The principal exception to this finding is that low-range, high-cross-range trajectories possess short-path-length parameters initially and transfer to long-path-length parameters once the turn is established. The qualitative relationship between E and time is the same for both 2- and 3-dimensional equations: the logarithm of E decreases nearly linearly with time, and the approximate slope is a function of the final path length. Flight times for the 15 trajectories vary from 434 to 692 sec.

Effects of Selected Parameter Variations

The previous results have used a single set of initial conditions, with constant mass and open final heading angle. The effects of increased initial velocity, positive initial γ , 10% mass increase, and constrained final heading angle are discussed in this section. In each of the above cases, a new $\alpha - \varphi$ set is computed. Initial condition perturbations also are applied with a fixed $\alpha - \varphi$ set, in order to evaluate the sensitivity of an optimal solution to initial condition errors. The reference trajectory for these runs has a final range of 350 nmi and cross-range of 50 nmi (cross-range = 0 for the constrained heading case).

Figure 8 presents altitude-velocity profiles for the first 3 variations. Increases in V_0 and γ_0 each tend to increase the path length of the trajectory, resulting in an early α increase and the altitude increase which is characteristic of distance-shortening trajectories. There is no significant change in the φ -profile as a result of the V_0 increase, but φ is about 5° greater during the altitude increase when $\gamma_0 = +3^\circ$. The H-V profiles for both cases have returned to the nominal profile by the time that altitude decreases to 100,000 ft. The 10% mass increase, which is representative of the return payload deviations that can be expected in normal operation, is dynamically identical to a 10% decrease in air density. The mass increase improves the vehicle's intrinsic ability to penetrate the atmosphere; thus an early α -increase is necessary to preserve a near-nominal H-V profile. The additional α is maintained to prevent an excessive q peak at $H = 125,000$ ft, causing this case to fall behind in reducing D_{go} . Consequently,

α must be reduced to improve L/D, causing the average q to increase and the H-V profile to drop below the nominal.

Specifying a non-zero final heading angle while constraining the end point to the initial plane of motion forces the ground track out-of-plane during the transition. There is a small reduction in early α as ϕ increases to provide the cross-range shown in Fig. 9. The roll reversal simultaneously brings cross-range back to a small value (there is a 1 nmi overshoot) and provides a 30° final heading angle.

If the initial conditions are varied without changing the control profile, there are appreciable variations in terminal position, maximum q, and maximum load factor, while the variations in V_f , γ_f , ξ_f and H_f are negligible. Typical variations in the latter are about 1 fps, $.1^\circ$, $.3^\circ$, and 10 ft for the initial condition variations shown in Table I, which compares the effects on round-earth trajectories. The excellent convergence of the terminal altitude and velocity vector is the result of scheduling α and ϕ as a function of E (and, therefore, H and V). Terminal position is not fed back by E-scheduling; therefore, its dispersion is significant (see Table I). Load factor and q peaks occur at the extremes of the trajectories. Altitude variation is seen to have the largest effect on these parameters.

Case	ΔR_f ,	ΔC_f ,	q_{\max} ,	Load Factor,
	nmi	nmi	psf	g's
Nominal (Flat-Earth)	.16	.26	187	1.9
Nominal(Round-Earth)	12.9	-1.6	177	2.
+500 fps	45.6	-6.6	176	2.2
-500 fps	17.3	3.3	178	1.7
+3 $^\circ$	31.3	-1.6	178	2.
-3 $^\circ$	-5.5	-1.2	176	2.
+5000 ft.	16.1	-1.7	175	1.6
-5000 ft.	9.4	-1.4	182*	2.4

* occurs at initial condition

Table I. Effects of initial condition variations on a transition to Range = 350 nmi, Cross-Range = 50 nmi. Maximum dynamic pressure occurs at the final point; maximum load factor occurs at the initial point.

A DYNAMIC PROGRAMMING APPROACH TO TRANSITION GUIDANCE

Up to this point, discussion has centered on 3-dimensional transition trajectories-- both the means of computing them and the results obtained for a particular vehicle and set of flight conditions. While these results define the flight environment during transition, they leave unanswered the question of guiding the vehicle during the actual flight, i. e., in "real-time." Simply choosing a single optimal set of $\alpha(E) - \varphi(E)$ is, of course, inadequate, as the vehicle must be guided to a terminal point which cannot be well-defined before the trajectory occurs. Furthermore, variations in atmospheric and vehicle characteristics and errors in deriving E from measurements of H and V could allow unacceptable dispersions in flight parameters. For the real-time case, some form of feedback guidance is mandatory.

There are 3 alternatives for optimal feedback guidance. The first is to execute a numerical optimization procedure, such as the one described in this paper, in conjunction with "fast-time integration" of the state and adjoint differential equations. Such a scheme has been devised for launch vehicles⁵ and has been suggested for entry guidance as well; this alternative was, in fact, the motivation for the current work. To date, however, the speed of convergence for the steepest descent/energy optimization described here, combined with the execution speed of foreseeable flight computers, is inadequate for real-time application to transition flight path control. The second alternative is to obtain neighboring extremal solutions for one or more optimal paths, resulting in a family of nominal state, control, and feedback gain histories for the linearized feedback guidance law. Linear control laws usually use time as the independent variable, but the present results indicate that specific energy is more appropriate. Perturbation guidance is most attractive if acceptable results can be achieved with a single nominal trajectory and set of feedback gains, for computer storage requirements are proportional to the number of nominal paths used. The examples of the previous sections suggest that 3 nominal paths would be required to adequately cover the transition footprint. The 3 cases would be long-distance, short-distance, and short-range/high-cross-range paths. The third alternative, which is explored in the remainder of this section, is dynamic programming. The principal distinction between this and the second alternative is that dynamic programming provides a nonlinear feedback law, eliminating feedback gains at the expense of more nominal paths.

A family of optimal transition trajectories constitutes an autonomous field of extremals which can be used for nonlinear feedback control. The theory of dynamic programming⁶ shows that a unique optimal control vector associated with each point in the extremal field can be defined. Hence, α and φ can be precomputed as optimal functions of these variables and stored within the flight computer. The present results suggest that two 3-parameter functions, in which the guidance commands (α_G and φ_G) are functions of D_{go} , A_{go} , and E only, are sufficient.

E - Guidance for Gliding Flight

A three-dimensional guidance scheme which uses nonlinear functions of D_{go} , A_{go} , and E to find α_G and φ_G is described, and closed-loop guidance results are presented in this section. As shown by Fig. 10, the nonlinear guidance functions are supplemented by dynamic-pressure-rate damping, in which α is modulated to minimize phugoid oscillations. The diagram shows that q' feedback brings in the state variables which are missing in the guidance functions (K and γ); in practice, q' also could be derived from measurement of \dot{V} .

The α_G and φ_G functions used for E (for "Energy") - Guidance are sketched in Fig. 11, with the A_{go} effects on α_G and the D_{go} effects on φ_G sketched as leaves of a multi-leaved guidance surface. In concept, α_G and φ_G follow the hypersurfaces defined by

$$\alpha_G = \alpha_G(D_{go}, A_{go}, E) \quad (65)$$

$$\varphi_G = \varphi_G(D_{go}, A_{go}, E), \quad (66)$$

although q' damping allows small variations as required. The same functions can be used to predict the terminal point which will result from the currently measured values of α and φ , using the revised form

$$D_{go P} = D_{go}(\alpha, \varphi, E) \quad (67)$$

$$A_{go P} = A_{go}(\alpha, \varphi, E) \quad (68)$$

The prediction assumes that an optimal α - φ profile is flown from the current point, and it neglects the effect of q' damping.

In the numerical results which follow, the guidance functions have been derived from the 15 optimal trajectories described earlier, with D_{go} and A_{go} determined from the actual terminal points obtained in round-earth computations; thus, the guidance functions terminate at the nominal specific energy with zero D_{go} and near-zero A_{go} . The guidance variables are constrained to the maximum and minimum tabulated values, which (for these cases) converge to functions of E alone as the end point is approached. Consequently, there are neither violent terminal maneuvers nor precise homing with the guidance functions used here. The most frequent result of these control constraints is that lateral position error is not completely nulled or that the terminal point is reached with surplus specific energy.

Table II lists the significant parameters of 7 round-earth trajectories to a range of 300 nmi and cross-range of 50 nmi using E-Guidance without trajectory damping. The first case has nominal initial conditions, while the remaining 6 cases have the initial condition perturbations used in Table I. In a departure from earlier convention, the terminal point is defined as the tabulated point of closest approach to the destination. As before, the maximum q and load factor occur at the end points.

	D_{go_f} ,	ΔE_f ,	V_f ,	q_{max} ,	Load Factor,
Case	nmi	ft	fps	psf	g's
Nominal	.84	701	850	168	2.1
+500 fps	.02	1290	858	169	2.4
-500 fps	.04	1593	855	165	1.5
+3°	.05	1241	846	162	2.1
-3°	.10	539	850	170	2.1
+5000 ft	.03	931	858	171	1.7
-5000 ft	.07	1231	860	182	2.6

Table II. Flight parameters for trajectories to 300-nmi range and 50-nmi cross-range using E-Guidance without trajectory damping.

Adding trajectory damping has little effect on the above-tabulated parameters, but it does smooth the flight path and dynamic pressure profiles. Figure 12 presents a comparison of E-Guidance flight paths with- and without dynamic-pressure-rate damping. The initial flight path angle is +3°, a condition which

provides substantial excitation of the phugoid mode. Dynamic-pressure rate is fed back to α with a constant gain of .04 until $E = 10^5$ ft; at this point, the gain is decreased to allow the dynamic pressure to build up to meet the terminal flight condition.

The most significant control change brought about by trajectory damping is the α pop-up at the beginning of transition. The initial α is sharply reduced to prevent phugoid excitation; once the peak altitude is reached, α closely follows the undamped profile. It can be concluded from this and previous results that the early maneuver, and not the continuing control, is more important in preventing large phugoid oscillations. Some oscillation does remain in the damped case, suggesting that higher feedback gain could be employed. The amount of damping demonstrated here reduces the maximum peak-to-peak load factor variation from 1.6 g to .4 g. Ranging control for the damped case is better than that of the undamped example, with a minimum tabulated D_{go} of .04 nmi and excess specific energy of 918 ft.

E-Guidance is relatively insensitive to vehicle mass or air density variation. A 10 % increase in vehicle mass decreases the maximum load factor accordingly and has negligible effect on maximum q . Terminal accuracy is adversely affected by the φ constraints of the guidance functions used here: the maximum final D_{go} for the 7 initial conditions considered previously is 1 nmi, although the average for the remaining 6 cases is .27 nmi.

The above results pertain to a low cross-range case; E-Guidance performs in much the same way when the terminal point is extended to the edge of the footprint (150-nmi cross-range at 300-nmi range). Table III indicates that

Case	D_{go_f} , nmi	ΔE_f , ft	V_f , fps	q_{max} , psf	Load Factor, g's
Nominal	.04	1346	852	176	1.5
+500 fps	.01	2169	850	174	2.1
-500 fps	69.02	—	822	251	1.3
+3°	.25	1700	849	191	1.4
-3°	.17	907	854	270	2.1
+5000 ft	.13	785	849	182	1.5
-5000 ft	.06	1370	852	191	1.6

Table III. Flight parameters for trajectories to 300-nmi range and 150-nmi cross-range using E-Guidance without trajectory damping.

terminal convergence is retained in all cases which have sufficient energy to reach the destination. The 11 % reduction in specific energy which results from an initial velocity perturbation of -500 fps prevents this case from meeting its objective.

φ^* Azimuth Control and α^* Distance Control

Two modifications to E-Guidance can be considered for the transition phase. The first makes use of the equilibrium relationship between φ and A_{go} which exists when A'_{go} is negligible; it is called φ^* azimuth control. The second evolves from the observation that the optimal α depends largely on path length rather than path curvature; it is called α^* distance control.

The roll angle φ^* is defined by eq. (31) as

$$\varphi^* = \sin^{-1}(-2 \sin A_{go} / D_{go} \cos^2 \gamma C_L k e^{-\beta H}) \quad (65)$$

Computing φ^* for the 4 extreme optimal trajectories presented in an earlier section, it is found that there is a close similarity between the optimal roll guidance command and φ^* . In general, the optimal φ is larger than φ^* , as the best control policy is to null A_{go} as the destination is approached rather than to maintain a constant A_{go} . Nevertheless, eq. (65) presents an explicit relationship between the state variables and the lateral control variable which need not be generated by numerical optimization; hence, it provides an attractive alternative to the optimal policy.

φ^* azimuth control is compared with the dynamic programming guidance function $\varphi_G(D_{go}, A_{go}, E)$ for high- and low cross-range in Fig. 13. Azimuth-to-go is kept very nearly constant by φ^* control (Fig. 13b), whereas the optimal A_{go} tends to zero. In the low cross-range case, however, the minimum miss distance is .84 nmi; as the vehicle flies past its destination, A_{go} diverges. Final D_{go} for the corresponding φ^* case is .03 nmi. Ground tracks for the high cross-range case, shown in Fig. 13a, show that optimality is important as the footprint boundary is approached. The optimal case reaches the destination with .04 nmi-error and a specific energy excess of 1346 ft, but the φ^* trajectory is 9.3 nmi from its goal when the final specific energy is reached. The roll angle profiles which provide these results are shown in Fig. 13c. Roll angle is limited to $\pm 45^\circ$, and each φ^* history reaches the limit. The limits on the optimal

guidance function, φ_G , are more severe as the end point is approached; hence, final lateral error is left uncorrected. For the low cross-range case, this causes large error in the optimal result, while the φ^* function goes to its limit to null the error. The early φ^* profile is inadequate in the high cross-range test, letting the lateral error build up to an uncorrectable level. This result suggests that φ^* control be revised to explicitly null the A_{go} which exists at the beginning of the trajectory. Allowing A'_{go} to be non-zero, the relationship for φ^* becomes

$$\varphi^* = -\sin^{-1} \frac{2}{C_L} \left[\frac{\sin A_{go}}{D_{go} \cos^2 \gamma k e^{-\beta H}} + C_D K A'_{go} \right] \quad (66)$$

The optimal results indicate that $\partial A_{go} / \partial \ln E$ is approximately constant during the transition; hence, choosing A'_{go} to be

$$A'_{go} = A_{go_0} / E(\ln E_0 - \ln E_f) \quad (67)$$

leads to an A_{go} profile similar to the optimal high cross-range case shown in Fig. 13b.

Simplification of the α guidance function proceeds from the fact that the rate-of-change of path length with respect to specific energy is independent of A_{go} ; therefore, the energy balance and ranging control obtained for planar motion are applicable to the 3-dimensional case. Since the time-rate-of-change of path length-to-go (PL_{go}) is just $-V$, eq. 11b becomes

$$\dot{D}_{go} = \dot{PL}_{go} \cos \gamma \cos A_{go} \quad (68)$$

which, for small γ , can be rewritten as

$$dPL_{go} = dD_{go} / \cos A_{go} \quad (69)$$

Equation 70 can be integrated by taking note of the fact that

$$\int f(y) dx = \int f(y) dy / (dy/dx) \quad (70)$$

or

$$\begin{aligned}
 \int d D_{go} / \cos A_{go} &= \int d A_{go} / [\cos A_{go} (d A_{go} / d D_{go})] \\
 &= \int d A_{go} / [C_D \mu (d A_{go} / d E)] \\
 &= \int d E / C_D \mu
 \end{aligned} \tag{71}$$

Taken between the appropriate specific energy limits, this is the integral form of eq. 35 when $A_{go} = 0$. This result justifies the use of PL_{go} as an input parameter for longitudinal control, but it does not solve the problem of determining PL_{go} in real-time; using eq. 71 to find PL_{go} requires integration of the remaining state equations to determine C_D and μ as functions of E . Fortunately, the constant- A_{go} assumption allows the horizontal flight path to be described by a simple spiral. Equation 69 is then readily integrated to yield

$$PL_{go} = D_{go} / \cos A_{go} \tag{72}$$

This relationship is exact for the original φ^* assumption. Figure 13a illustrates that the path length of the constant- A_{go} trajectory is greater than the optimal path length; hence, eq. 72 provides a conservative (long) path length estimate for guidance. α^* distance control is then defined by the 2-parameter guidance function

$$\alpha^* = \alpha^* (PL_{go}, E) \tag{73}$$

In summary, E-Guidance evolves from numerical trajectory optimization through real-time dynamic programming of the 2 control variables to φ^*, α^* control with q' damping. In the final, simplified form, energy balance and path length control are obtained by α modulation, which is based on a nonlinear guidance surface and linear feedback of the dynamic-pressure rate. The dynamic programming guidance surface can be obtained by numerical optimization of the planar case, as only path length and specific energy determine the angle of attack. Roll control of cross-range derives from an analytical function (eq. 66 and 67) which combines E, α (through C_L and C_D), and all of the state variables.

CONCLUSION

Computation of optimal gliding trajectories for the space shuttle transition is facilitated by making several transformations to the original, 3-dimensional set of dynamical equations. Introduction of total energy, kinetic energy, and polar position coordinates leads to a simpler description of the spacecraft's motion. This aids the optimization process and establishes a natural set of components for the guidance solution. The change of variables provides a fixed end-point for the transition trajectory without restricting the final time and leads to a proportional guidance law (ϕ^* control) for the lateral state. As presented, the equations also are applicable to terminal area maneuvering and landing approach, and the equations could be extended to hypersonic entry with little difficulty.

Numerical results indicate that a wide range of α profiles is required to fly to representative points within the transition footprint. If there is any concern for meeting flight path constraints without restricting ranging capability, the concept of a single α -profile for transition must be rejected. Similarly, the notion of a discrete transition from the back-side of the L/D curve (i. e. , from an α greater than that required for maximum L/D) to the front-side to minimize flight loads or to preserve ranging control is falacious. If dynamic pressure and load factor peaks are to be minimized, C_L must be kept as large as possible; therefore, α should be reduced to cruising flight values just prior to initiating the terminal-area maneuvering phase. The discrete α -jump from one side of L/D_{\max} to the other is also seen to be detrimental for the case of maximum-range flight; in such an instance, L/D must be maximized during the entire entry/cruise transition. As demonstrated here, ranging control is not dependent on maintaining a quasi-linear relationship of known magnitude and sense between L/D and α ; rather it depends on a knowledge of specific energy, distance-to-, and direction-to the destination. There are, however, valid reasons for performing a discrete α -jump during the space shuttle transition. Static instability motivated a previous study of such jumps², and a recent study of unsteady aerodynamics suggests that leeside shock-induced separation, sudden leading-edge stall, and vortex burst may force such a maneuver to be reconsidered.⁷

The concept of dynamic programming provides a rigorous link between the optimal results and a practical realization for transition guidance. The "curse of dimensionality" which haunts dynamic programming would appear to obviate such an approach to transition guidance, for both α and ϕ would be 6-parameter functions in the 3-dimensional case; however, the demon is exorcised by the facts that 2 states (ξ and η) always enter the problem in combination (A_{go}) and 2 states (K and γ) contribute primarily to phugoid-mode damping. The α and ϕ

guidance functions are, therefore, readily expressed as 3-state hypersurfaces; these can be augmented by feedback of the remaining 2 states for trajectory damping. Dynamic programming in reduced dimension thus forms the basis for E-Guidance.

The E-Guidance formulation is further simplified by incorporating a near-optimal guidance law for lateral motion (ϕ^* azimuth control) and by replacing D_{go} and A_{go} by PL_{go} in the angle-of-attack guidance function (α^* distance control). Nonlinear, explicit guidance for the space shuttle transition provides flight paths similar to the optimal trajectories with substantially reduced computation.

A final point of some operational significance is the use of the E-Guidance functions to predict the instantaneous destination and footprint for crew displays. Whether the spacecraft is under manual control or is being flown automatically, the pilot must be able to evaluate the progress of the flight and the limits of maneuverability imposed by the current energy-state. The predictive computation required to generate this information can easily exceed the actual guidance logic. The E-Guidance functions can be inverted to provide this prediction from measured values of α , ϕ , and E at little additional computational cost.

REFERENCES

1. Stengel, R. F. , "Energy Management During the Space Shuttle Transition," CSDL Report E-2708, (presented at the AIAA 2nd Atmospheric Flight Mechanics Conference, Palo Alto, Sept. , 1972).
2. Stengel, R. F. , "Strategies for Control of the Space Shuttle Transition," AIAA Paper No. 71-921, New York, 1971, (to be published in Journal of Spacecraft and Rockets).
3. Click, P. L. , Michna, D. J. , Sarver, D. A. , "Aerodynamic Stability and Control Characteristics of the NASA/MSX .006 Scale 040-A Delta Wing Orbiter," NASA CR-120015, Huntsville, Nov. , 1971.
4. Deyst, J. J. , Gustafson, D. E. , Kriegsman, B. A. , "Optimal Lateral Guidance for a Low L/D Shuttle Vehicle Entry," AIAA Paper No. 71-914, New York, 1971.
5. Baker, C. D. , Causey, W. E. , Ingram, H. L. , "Mascot - A New Concept in Guidance," NASA TMX- 64573, Huntsville, March, 1971.
6. Bellman, R. , Kalaba, R. , "Dynamic Programming and Adaptive Processes," IRE Transactions on Automatic Control , Vol. AC-5, No. 1, Jan. , 1960, pp. 5-10.
7. Reding, J. P. , Ericsson, L. E. , "Delta Wing Separation can Dominate Shuttle Dynamics," AIAA Paper No. 72-976, Palo Alto, Sept. , 1972.

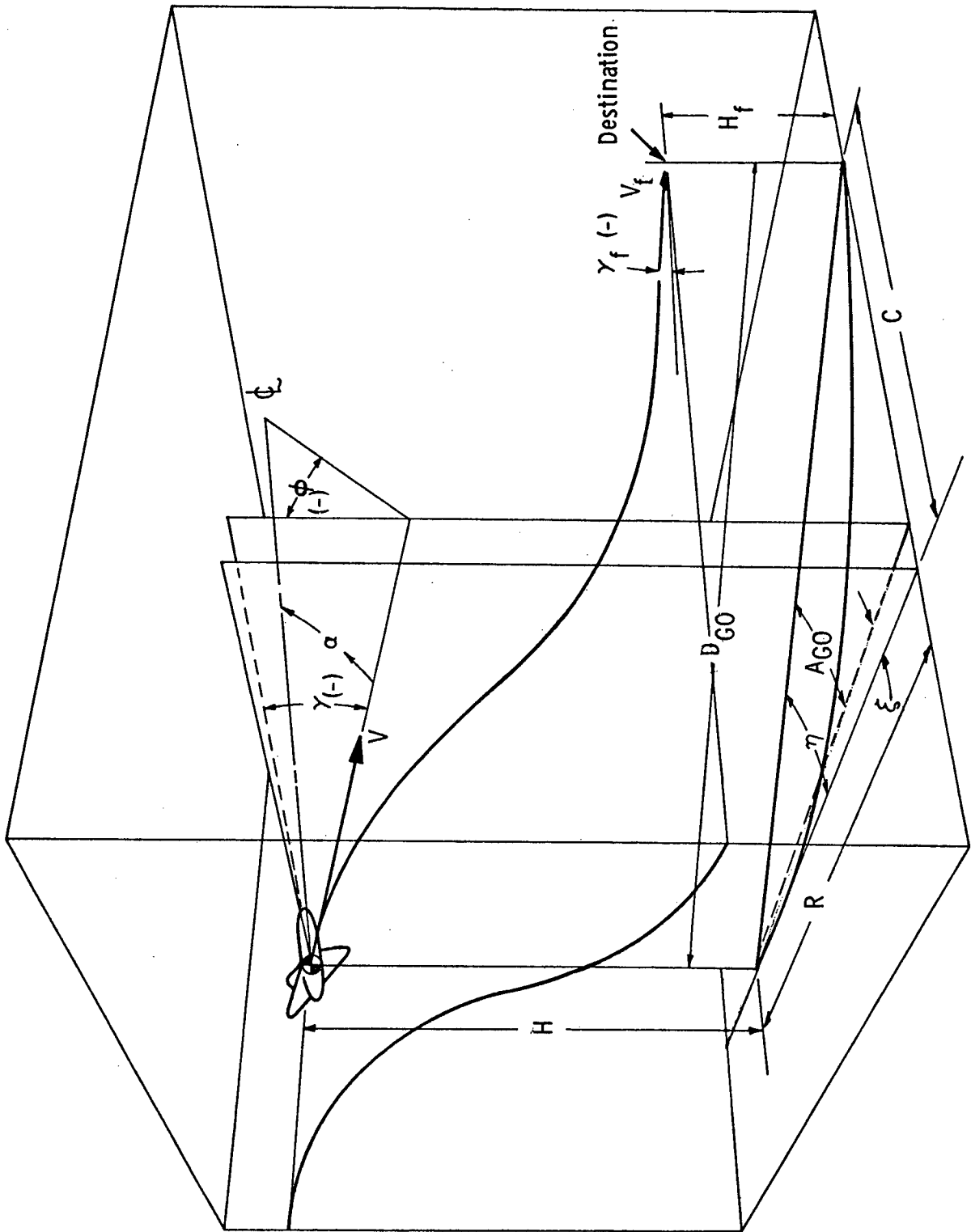


Figure 1. Coordinate System for the Space Shuttle Transition.

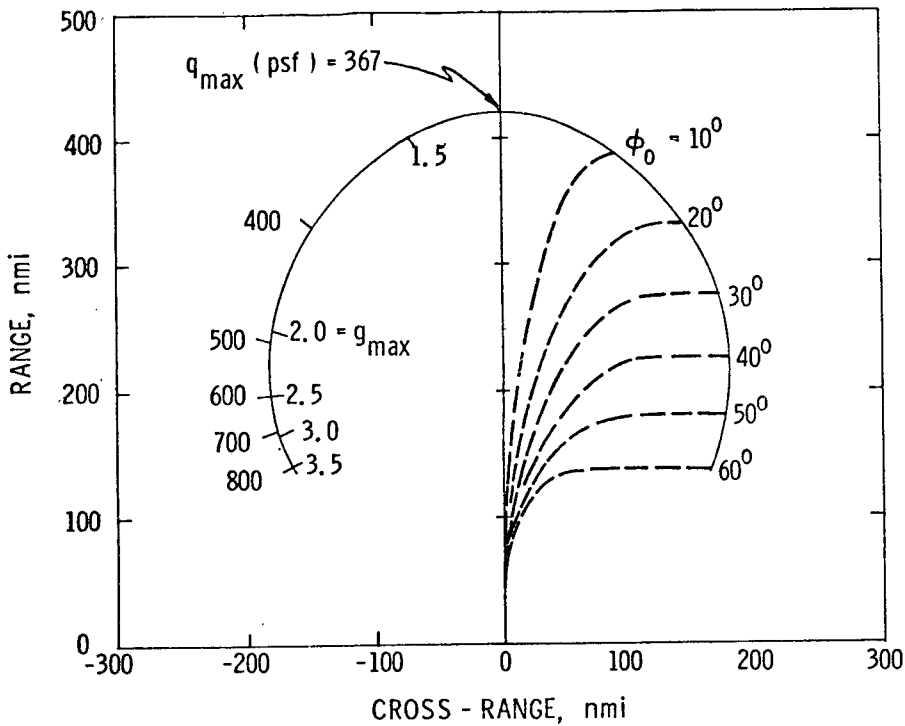


Figure 2. "Footprint" for flight at L/D_{max} (Round-Earth). Constant Roll Angle held until 90° heading is reached; then roll angle = 0° . Ground track shown by dashed lines. Maximum dynamic pressure (q_{max}) and load factor (g_{max}) shown as a function of terminal point. $V_0 \approx 800$ fps, $H_0 \approx 41,500$ ft.

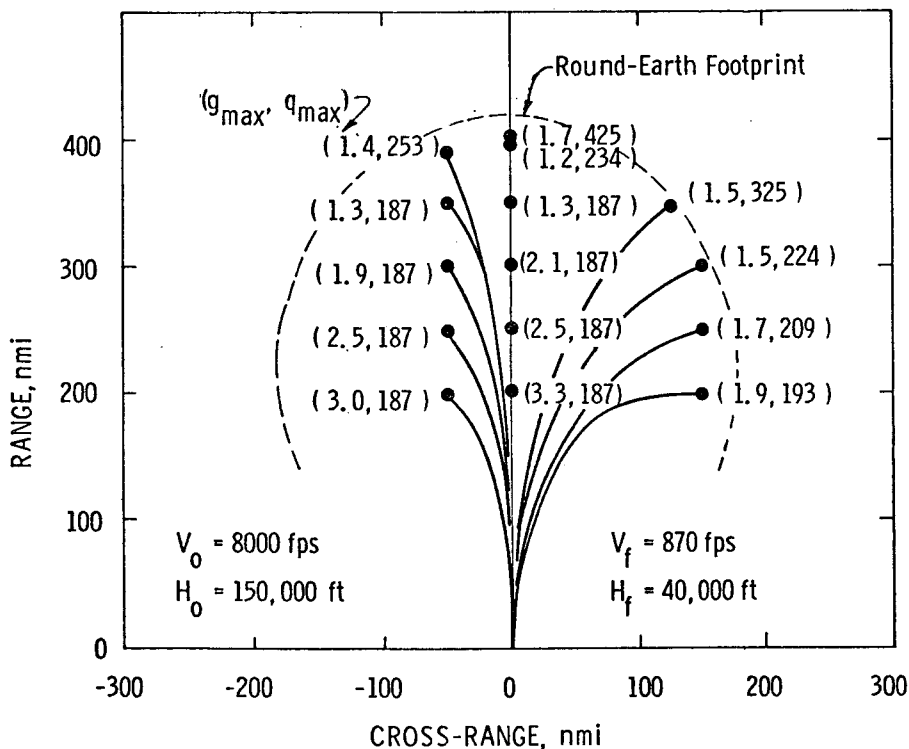


Figure 3. Ground tracks of 15 transition trajectories calculated with flat-earth assumptions. Maximum load factor (g 's) and dynamic pressure (psf) shown in parentheses next to each terminal point.

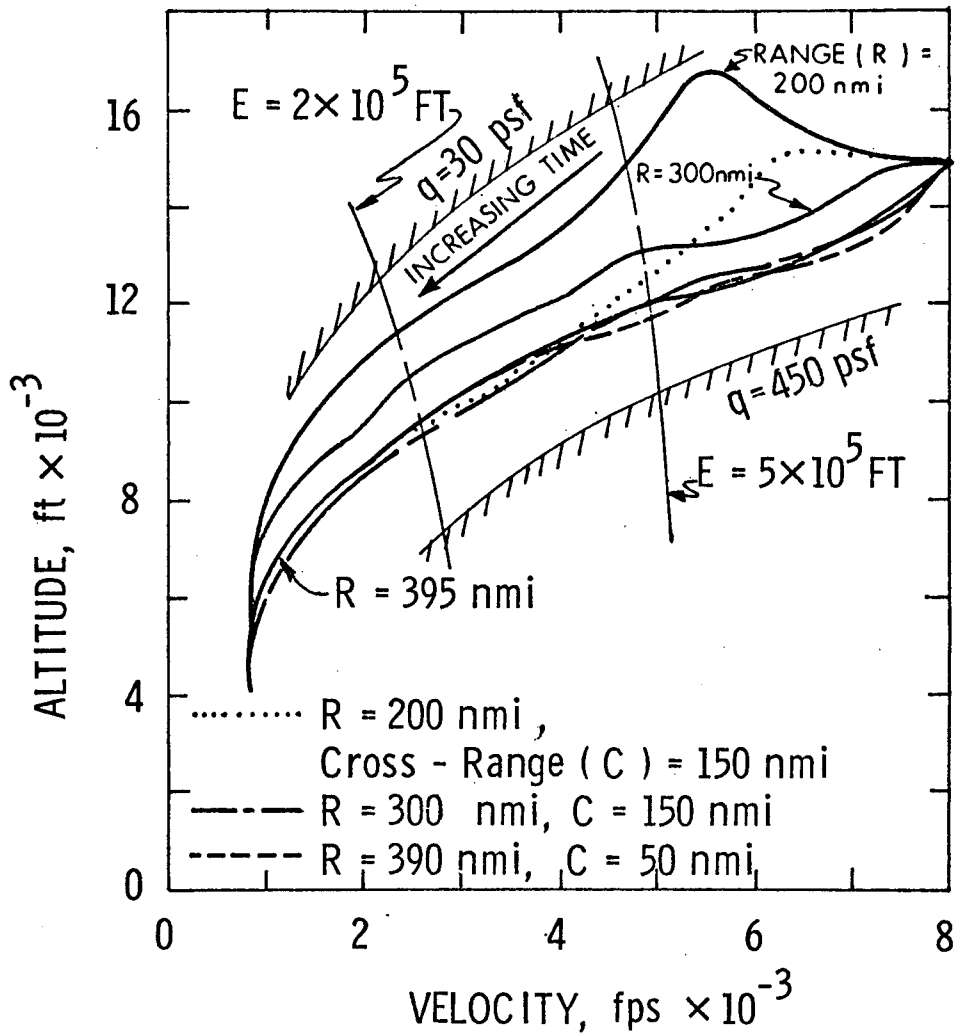
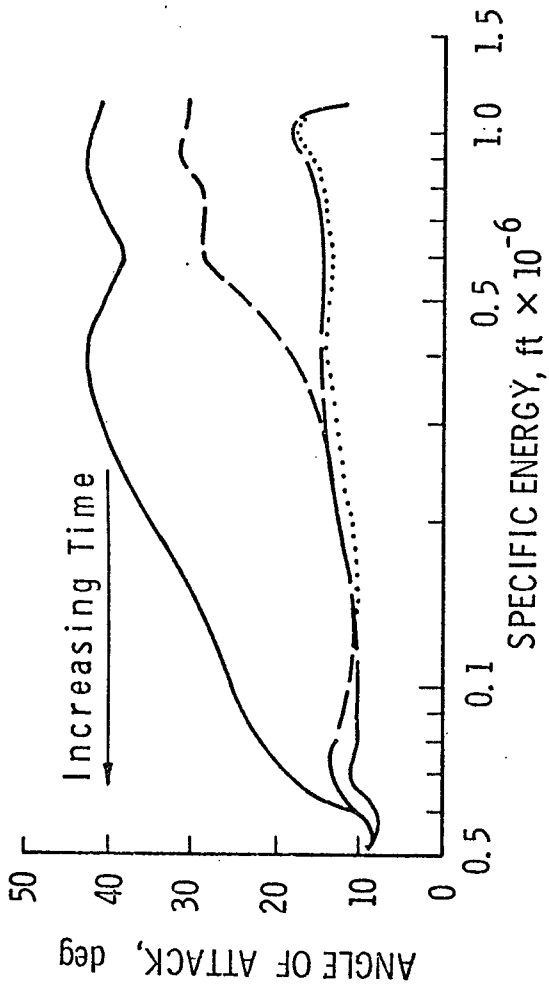
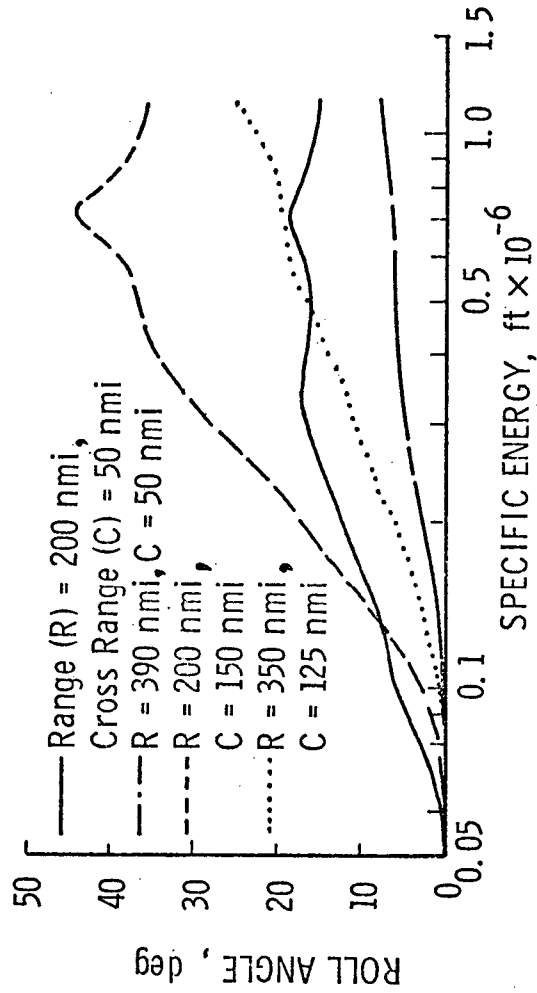


Figure 4. Altitude-Velocity profiles for several transition trajectories. Short range trajectories require early deceleration and, therefore, high α . This leads to an initial increase in altitude. Long path-length trajectories require high kinetic energy at a fixed level of specific energy; hence, dynamic pressure is higher.

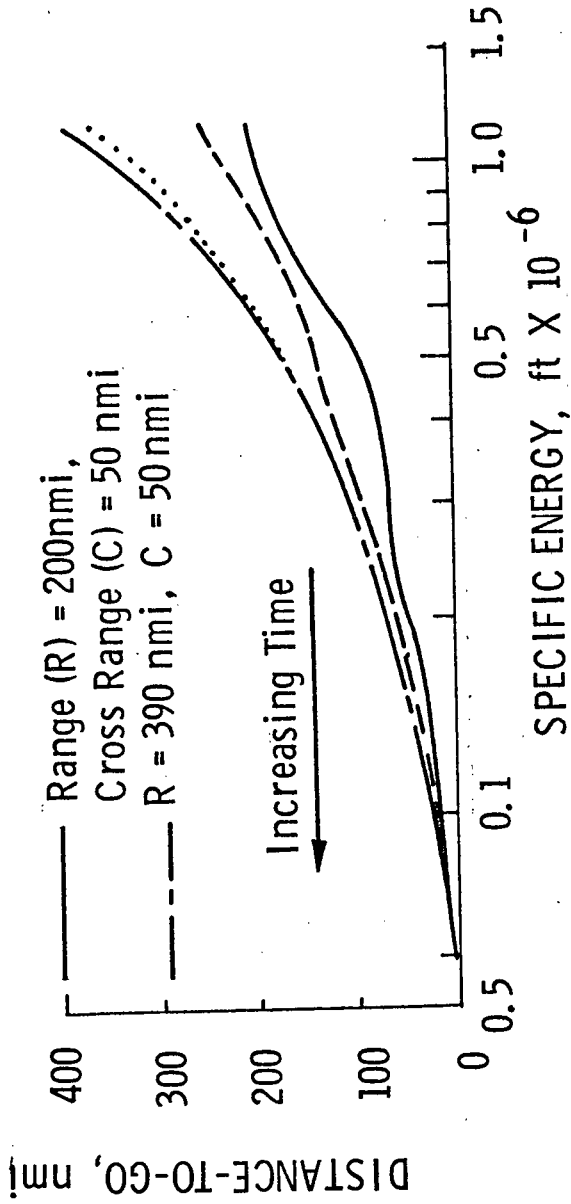


a) Angle-of-Attack History

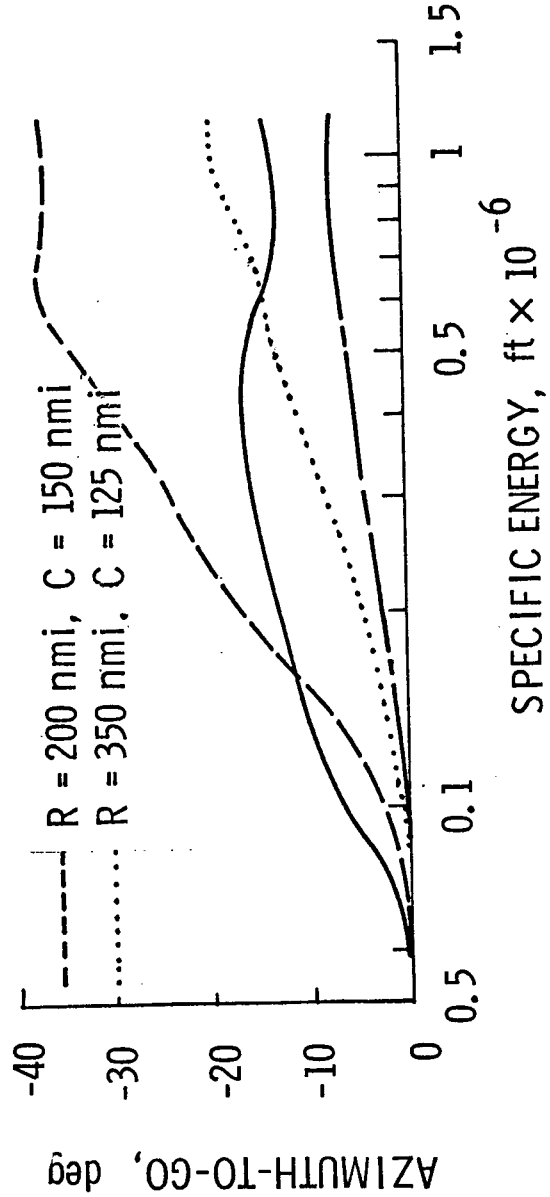


b) Roll Angle History

Figure 5. Control histories for 4 transition trajectories. Angle-of-attack (α) trends can be related to the H-V trends seen in the previous figure. Reference to the next figure indicates that roll angle (ϕ) is a straight-forward function of azimuth-to-go.

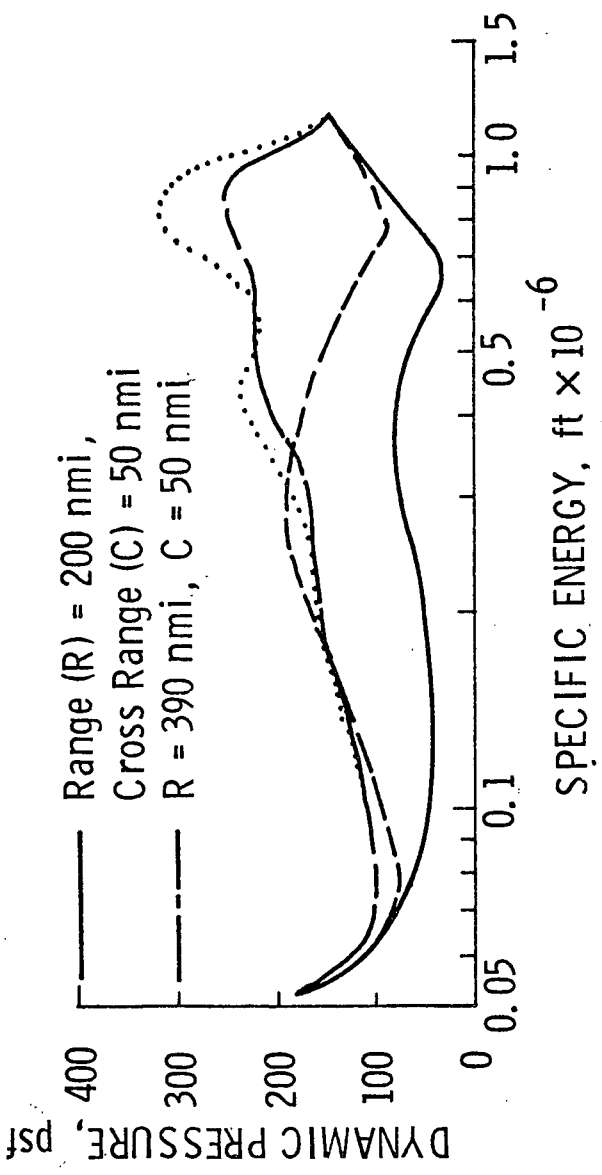


a) Distance-to-go History

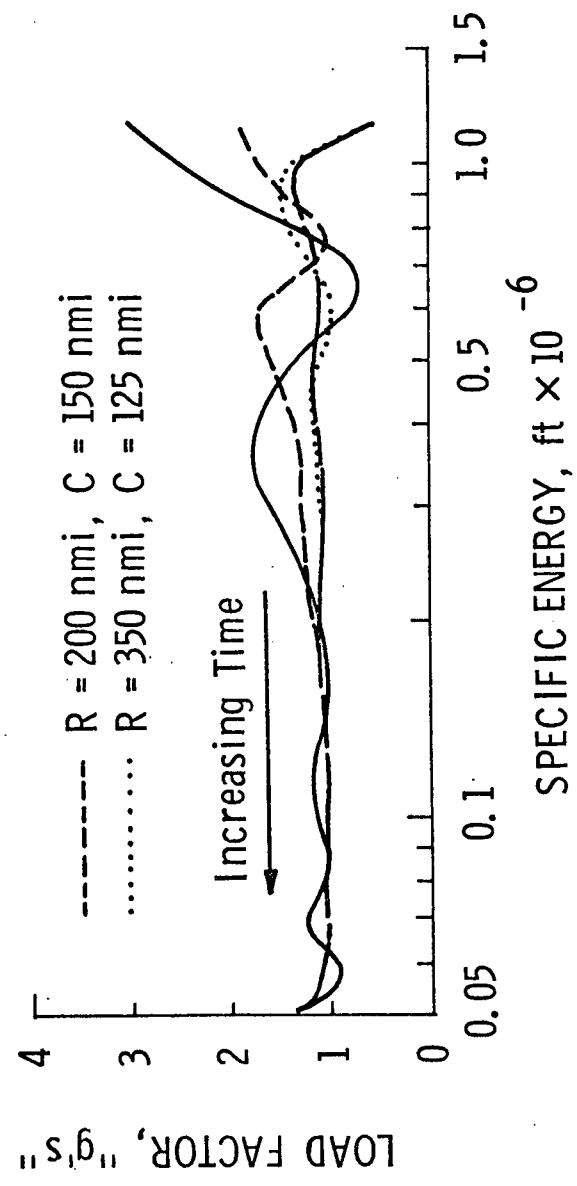


b) Azimuth-to-go History

Figure 6. Position histories for 4 transition trajectories. Distance-to-go (D_{go}) trends are similar to the H-V and α trends of previous figures. The convergence of azimuth-to-go (A_{go}) indicates a "straight-in" final approach to the destination.



a) Dynamic Pressure History



b) Load Factor History

Figure 7. Dynamic variables for 4 transition trajectories. Maximum dynamic pressure (q) is associated with the terminal point for short-distance cases. Maximum load factor generally occurs near the beginning of the transition.

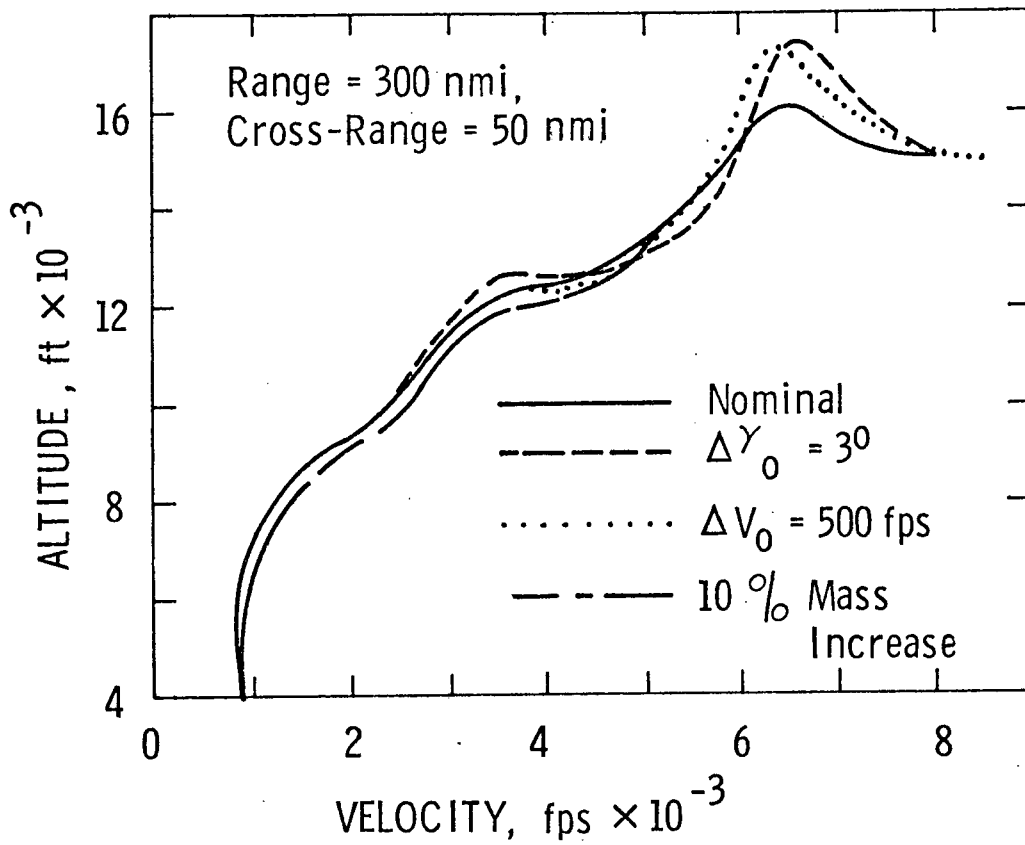


Figure 8. Optimal H-V profiles for initial flight path angle (γ), initial velocity (V), and mass variations.

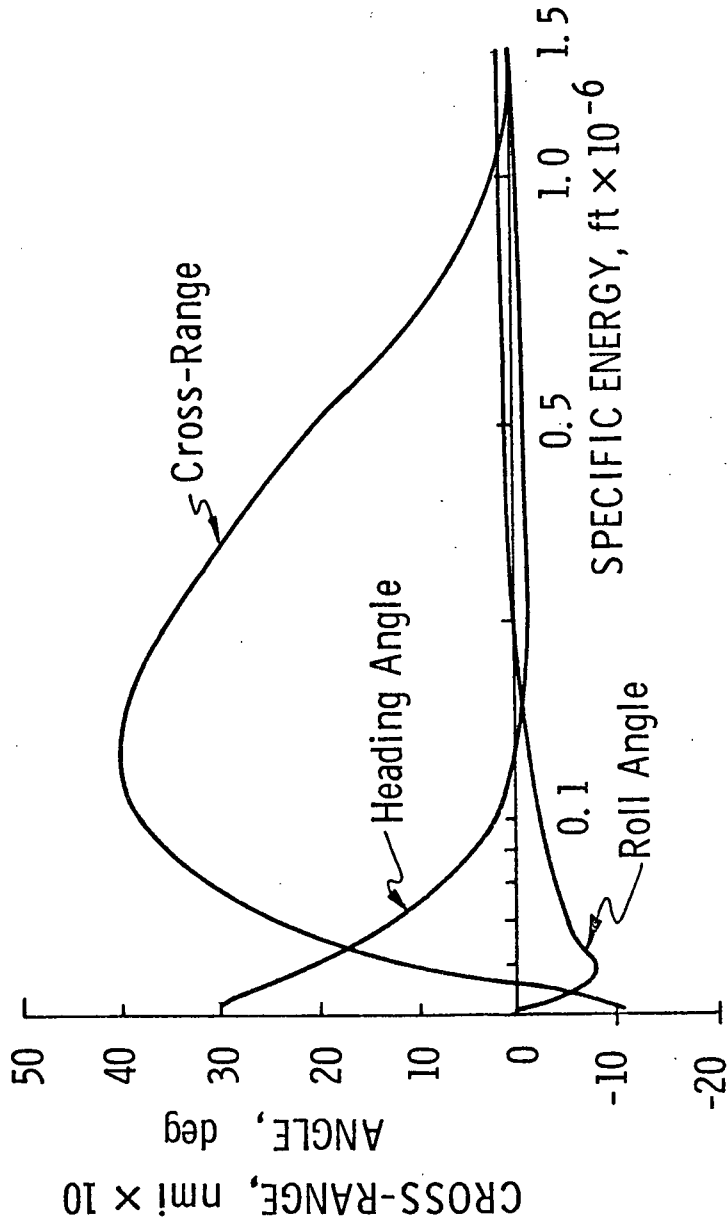


Figure 9. Parameters for a 350 nmi-range transition with final heading angle constrained to 30°. Vehicle moves out-of-plane to minimize final cross-range.

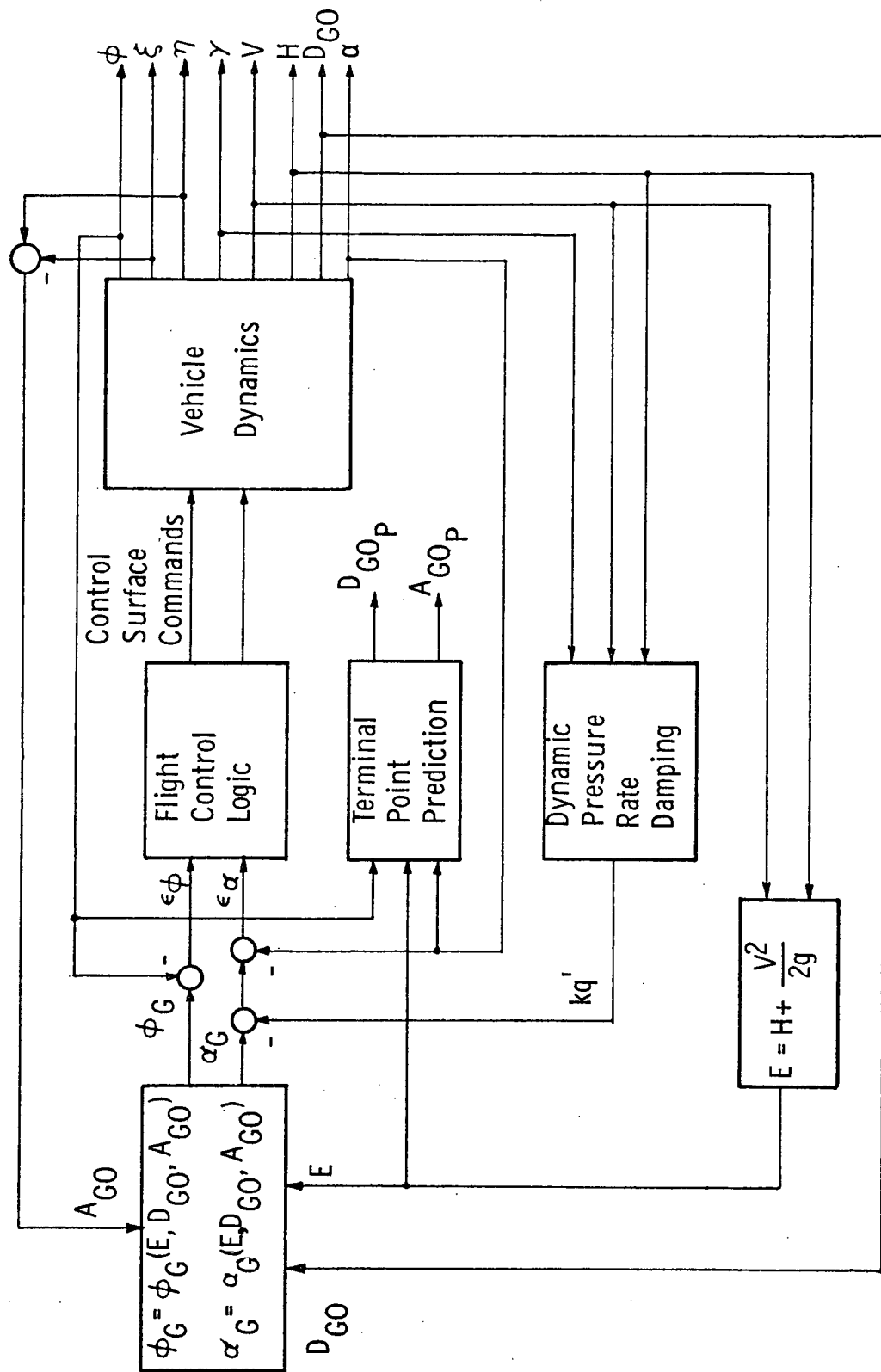
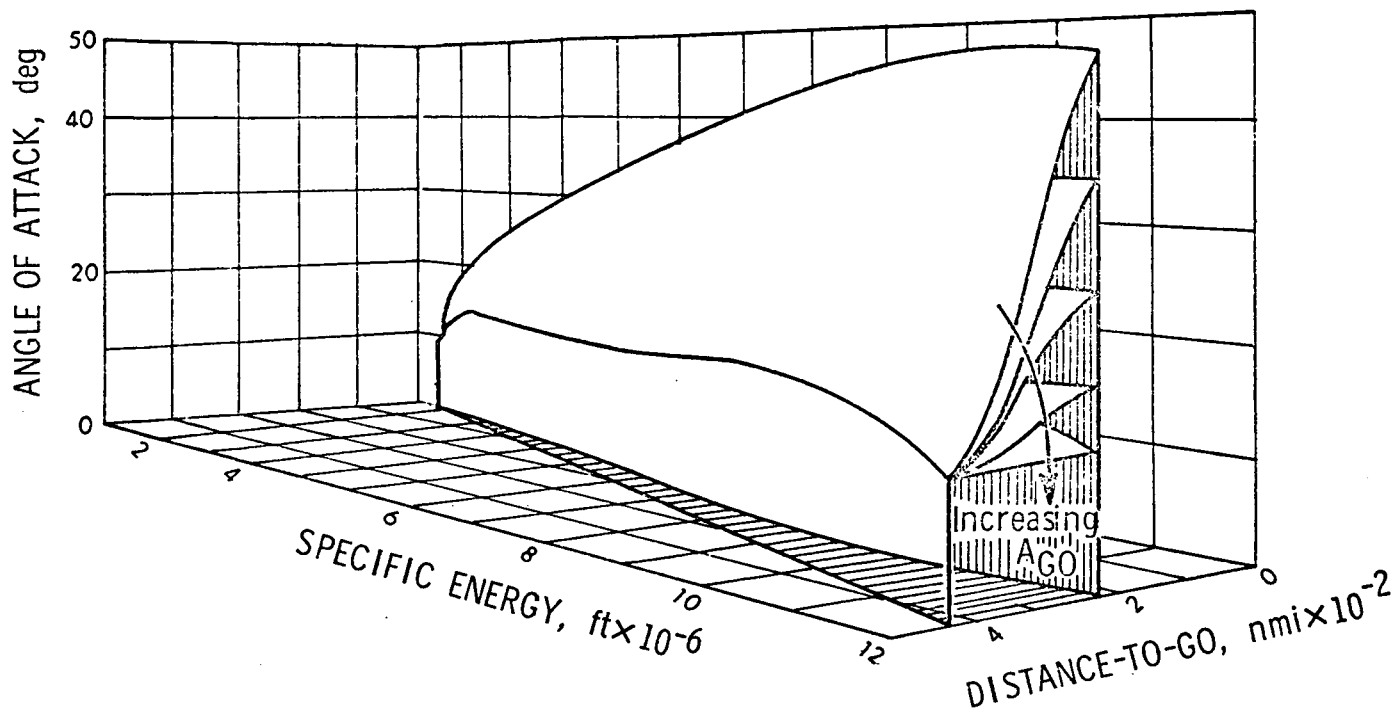
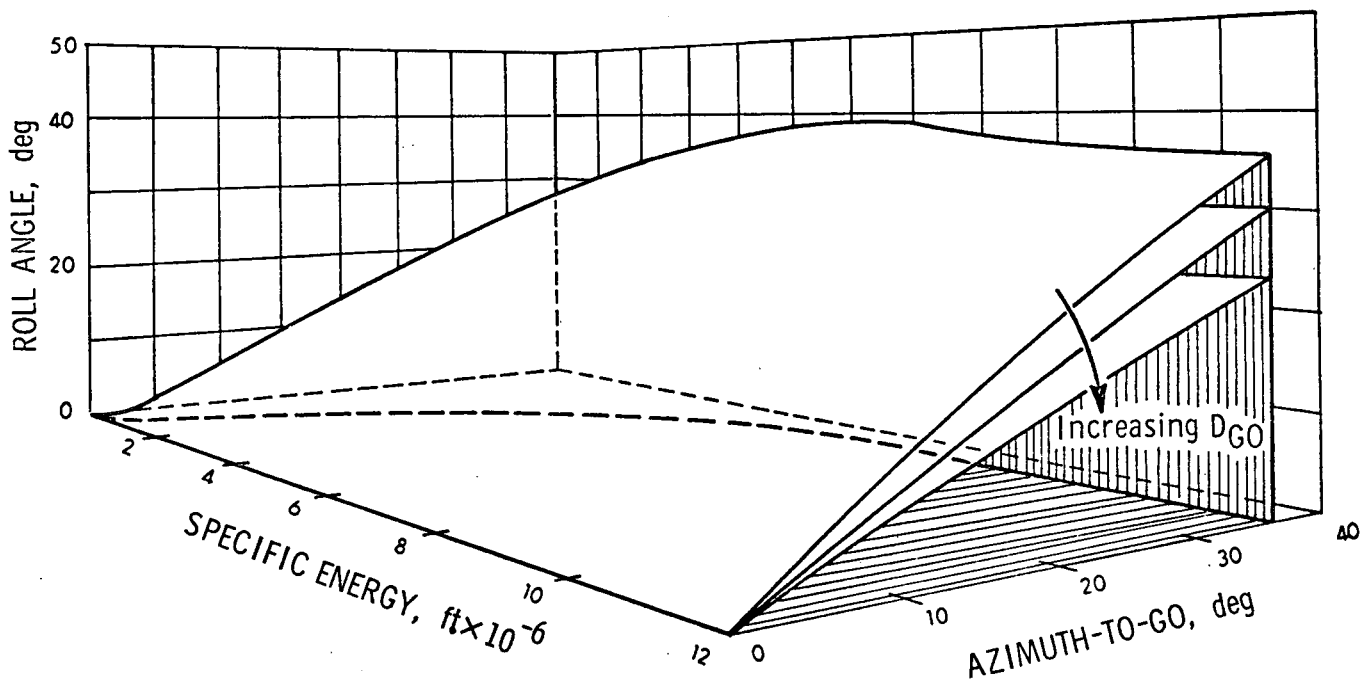


Figure 10. Block diagram of the E-Guidance Law for gliding flight.

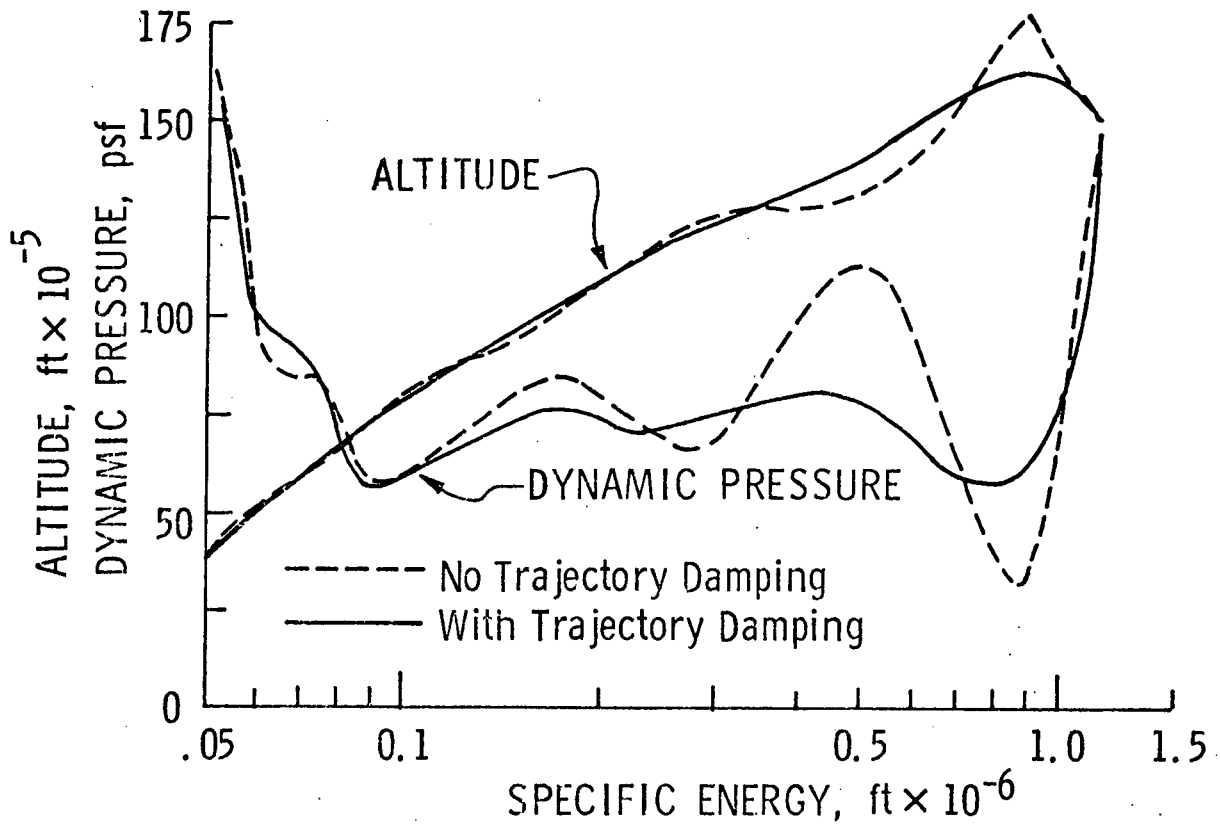


a) α guidance function

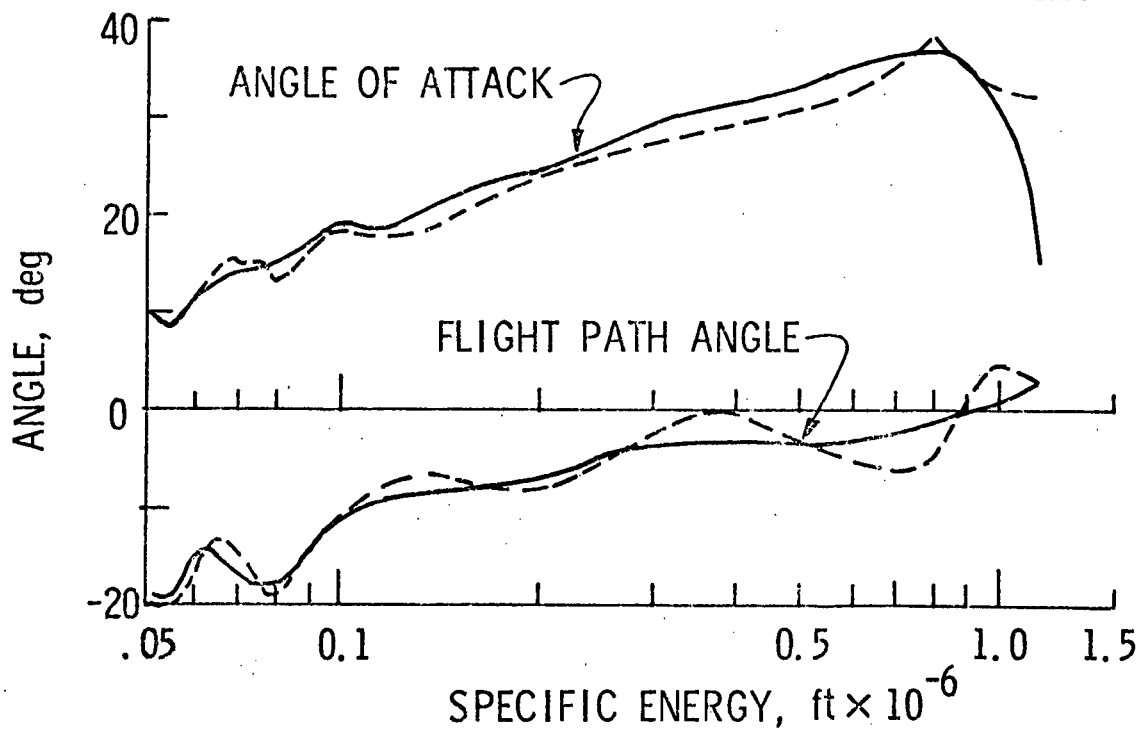


b) ϕ guidance function

Figure 11. **E**-Guidance functions for the space shuttle transition.



a) Altitude and Dynamic Pressure Histories



b) Angle of Attack and Flight Path Angle Histories

Figure 12. The effects of dynamic-pressure-rate (q') damping on a typical, guided trajectory. The phugoid oscillation established by an initial γ of 3° is reduced when α is modulated by a linear feedback of q' .

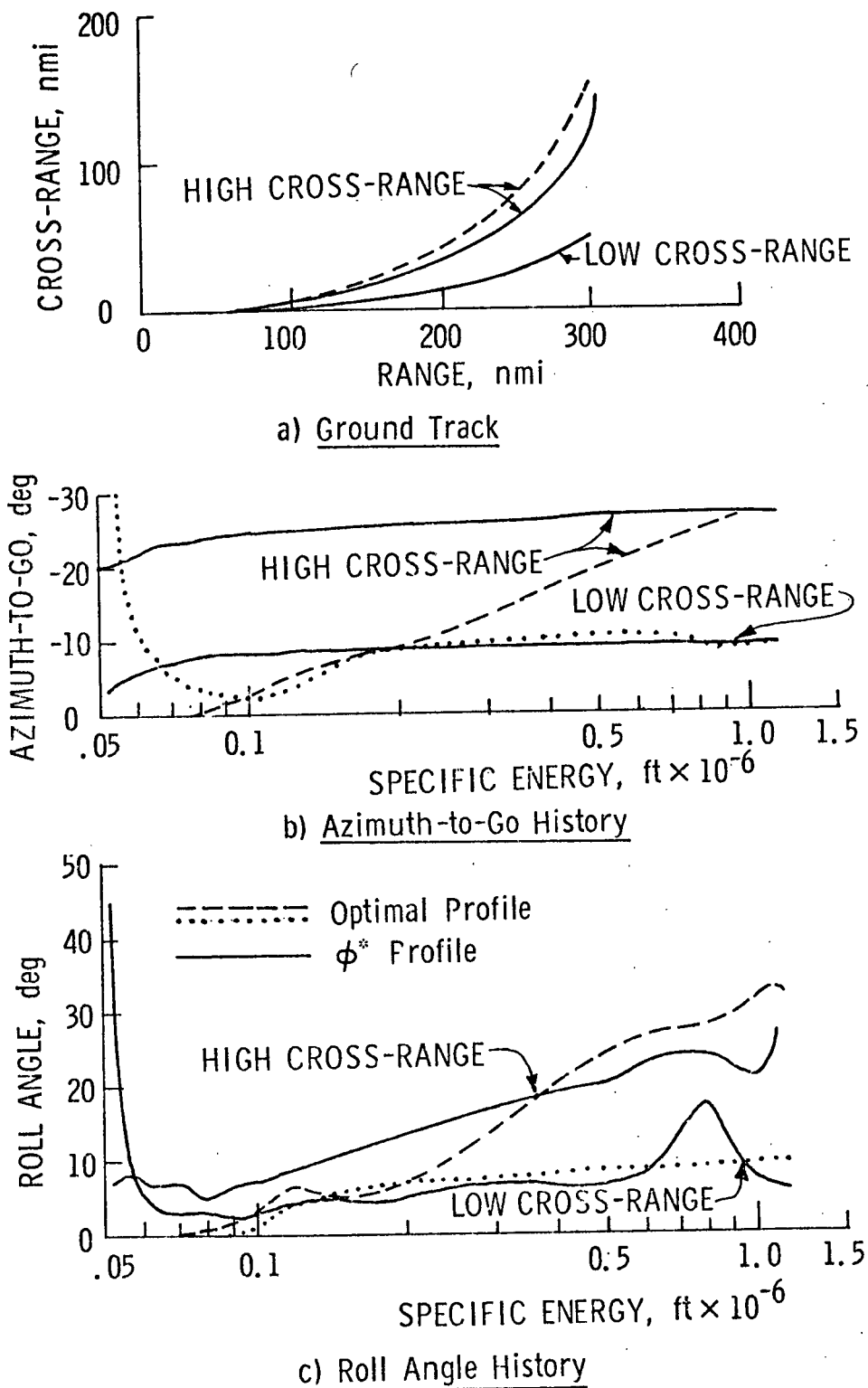


Figure 13. A comparison of optimal azimuth control and ϕ^* azimuth control for high- and low cross-range trajectories. The constant A_{go} of the ϕ^* , high cross-range case increases path length to the destination, and, therefore, the energy required. E_o is insufficient to reach the destination in this case. Low cross-range convergence with constant A_{go} control is very good.

DISTRIBUTION LIST

Internal:

R. Battin
 H. Blair-Smith
 T. Brand
 A. Cook
 R. Cushing
 J. Deyst
 A. Engel
 G. Edmonds
 P. Felleman
 T. Fitzgibbon
 J. Gilmore
 F. Glick
 D. Gustafson
 E.J. Hall
 M. Hamilton
 J. Harper
 D. Hoag
 L. Johnson
 M. Johnston
 J. Kernan
 A. Klumpp
 G. Kossuth
 B. Kriegsman
 J. Laning
 G. Levine
 T. Edelbaum
 A. Hopkins
 P. Mimno
 E. Muller
 J. Nevins
 J. O'Connor
 E. Olsson
 G. Ogletree
 R. Ragan
 W. Robertson
 N. Sears
 G. Silver
 R. Stengel (75)
 G. Stubbs
 R. Weatherbee
 Apollo Library (2)
 CSDL Library (10)
 SSV Central Files (4)
 D. Fraser
 D. Gustafson
 Group 23C (25)

External:

NASA/RASPO (1)
 Delco (3)
 Kollsman (2)
 Raytheon (2)
 MSC:
 National Aeronautics and Space Administration (32 & 1R)
 Manned Spacecraft Center
 Houston, Texas 77058
 Attn: Apollo Document Control Group
 (BM 86) (18 & 1R)
 R. Chilton
 K. Cox (3)
 W. Peters (3)
 J. Hanaway
 F. Elam
 G. Zacharias
 W. Bradford
 S. Mann
 J. Williams
 T. Price
 KSC:
 National Aeronautics and Space Administration (1R)
 J.F. Kennedy Space Center
 J.F. Kennedy Space Center, Florida 32899
 Attn: Technical Document Control Office